Donor-Acceptor Truxene-Based Porous Polymers: Synthesis, Optoelectronic Characterization and Defense-Related Applications

Nayara Méndez-Gil, Sergio Gámez-Valenzuela, Marcelo Echeverri, Gary H. Suyo, Marta Iglesias, M. Carmen Ruiz Delgado,* and Berta Gómez-Lor*

Four donor-acceptor (D-A) polymers are synthesized by combining two different electron donors (truxene and its more electron rich triaza analogue, triindole) with an electron-deficient monomer (benzothiadiazole) through two different positions (2,7,13 or 3,8,13) and their optoelectronic properties are studied by theoretical and experimental methods. One of the polymers exhibits remarkable sensing capabilities for explosive nitraoaromatics while another demonstrated efficient photocatalytic activity in the aerobic sulfoxidation of the sulfur mustard simulant 2-chloro-ethyl ethyl sulfide (MGS) sulfoxidation. These results highlight their potential applications in defense-related areas. Moreover, the structure-performance relationships observed among the four polymers have enabled us to deepen the understanding of the mechanisms underlying the performance of these polymers in the aforementioned applications, thereby providing valuable insights to further improve their properties.

1. Introduction

The recent upsurge of terrorist activity has made the rapid, selective and sensitive detection of explosives one the most critical issues concerning national security and environmental safety.[1]

N. Méndez-Gil, M. Echeverri, G. H. Suyo, M. Iglesias, B. Gómez-Lor
Instituto de Ciencia de Materiales de Madrid
CSIC
C/ Sor Juana Inés de la Cruz, 3, Madrid 28049, Spain
E-mail: bgl@icmm.csic.es
S. Gámez-Valenzuela, M. C. R. Delgado
Department of Physical Chemistry
University of Málaga
Campus de Teatinos s/n, Málaga 29071, Spain
E-mail: carmenrd@uma.es
G. H. Suyo
Universidad San Francisco Xavier de Chuquisaca
Sucre Bolivia

Likewise, the transformation of chemical warfare agents into less toxic compounds has become a main concern of governs.[2] For both applications conjugated microporous polymers (CMPs) with their convenient chemical modularity, remarkable thermal chemical stability and persistent porosity have recently emerged as highly promising candidates.[3,4] On the one hand, the luminescent properties of these π-extended materials have been successfully used to detect analytes of interest on the base of enhanced electronic and optical responses.[5] On the other hand, the interaction of their π-conjugated systems with light are in the base of the photocatalytic detoxification activity which have been demonstrated by novel semiconducting porous polymers.[6,7]

For the performance of these materials in optoelectronics and catalysis, the position of the HOMO and LUMO energy levels and their bandgap energy are of fundamental importance.[8] These factors can be conveniently tuned through the adequate choice of the constituent monomers, the linking groups that connect them and their linkage position. On the other hand, the alternation of donor and acceptor building units in the polymeric skeleton have been found to be a powerful strategy to enhance the absorption capability and fluorescence efficiency of these materials, with strong implications for their light harvesting ability, their emission properties or their charge carrier recombination characteristics.[9]

The synthesis of these polymers has been approached using a wide array of protocols, spanning from metal-catalyzed cross-coupling reactions (Suzuki, Yamamoto, Sonogashira, Heck, etc.), polycondensations mediated by Lewis acids (Scholl, oxidative coupling, Friedel-Crafts, etc) to acid-catalyzed trimerizations. Significant synthetic efforts are also devoted to obtaining these porous materials through more environmentally friendly methods, such as microwave activation or mechanochemistry.[10] Interestingly, although the use of mechanical activation to promote a wide variety of chemical reactions has been already demonstrated,[11–16] its application to porous polymer synthesis has been predominantly limited to Friedel-Crafts polymerization.[17–20]

We have previously reported different truxene-based polymers that show interesting photocatalytic activity in reactions

ADVANCED
SCIENCE NEWS

www.advancedsciencenews.com

ADVANCED
FUNCTIONAL
MATERIALS

www.afm-journal.de

such as water splitting, oxidative photodegradation or amines homocoupling.[21–23] We have also found that truxene-based polymers can be used as sensors of nitroaromatic compounds through a fluorescence quenching mechanism and have established that the connectivity position of the monomers has important implications for their sensing capability.[24]

In an attempt to optimize the performance and move towards practical application of truxene-related polymers, in this manuscript we introduce four new donor-acceptor polymers synthesized by connecting electron-rich semiconducting C_3-symmetric truxene monomers or its triaza triindole analog with an electron-deficient C_2-symmetric benzothiadiazole (BTD) co-monomer, either through the 2,7,13 or 3,8,13 positions. By following this strategy, we have successfully influenced their frontier energy levels, thereby impacting their photocatalytic activity, as well as their emission properties and the mechanism governing their sensing performance. Interestingly, the synthesis of the four polymers was carried out by cross-coupling methodology under microwave or mechanical activation, thus providing an environmentally friendly protocol to access these new polymers.

2. Results and Discussion

2.1. Synthesis and Characterization

The synthesis of the monomers 2,7,12-tribromohexamethyltruxene (**Tx2Br**) and 3,8,13-tribromohexamethyltruxene (**Tx3Br**) was performed in just two steps starting from commercially available 6- and 5-bromoindanone in ACOH/HCl followed by methylation with MeI as previously reported.[25] Triindole **Tri2Br** and **Tri3Br** monomers were obtained by trimerization of 6- and 5-bromo-1-methylindolin-2-one in refluxing POCl$_3$.

Truxene- and triindole-based **Tx2-BTD Tx3-BTD**, **Tri2-BTD** and **Tri3-BTD** CMPs, were obtained by carbon-carbon Suzuki-Miyaura cross-coupling reaction between the corresponding tribrominated monomers and 4,7-bis(4,4,5,5-tetramethyl-1,3,2-dioxaborolan-2-yl)benzo[c][1,2,5]thiadiazole under microwave activation (see **Scheme 1**, **Figure 1**). After filtration and exhaustive washing with H$_2$O, aqueous diluted acids, acetone, dichloromethane (DCM), diethyl ether, and finally treatment with KCN in a mixture acetone/H$_2$O to remove the residual palladium(0). **Tx2-BTD and Tx3-BTD** were obtained in 85 and 64% yields as yellowish powders, while **Tri-2BTD** and **Tri3-BTD** were obtained in 71 and 90% as dark-brown powders. Interestingly, the cross-coupling reactions could be conducted in a ball-mill by mechanosynthesis. This approach drives to polymers with very similar electronic properties albeit with slightly lower yields (50% for **Tx2-BTD**, 31% for **Tx3-BTD**, 71% for **Tri-2BTD** and 98% for **Tri3-BTD**).

The chemical composition of the polymeric solids was investigated by elemental analysis, Fourier transform infrared (FT-IR) and solid-state ^{13}C cross polarization magic angle spinning (CP/MAS) NMR. Elemental analysis of the synthesized polymers shows experimental data for C, H, N, and S slightly lower than those calculated, which is common in porous polymers because some residual occluded solvent in the pores or incomplete combustion of the polymers. However, the carbon/nitrogen ratio is in
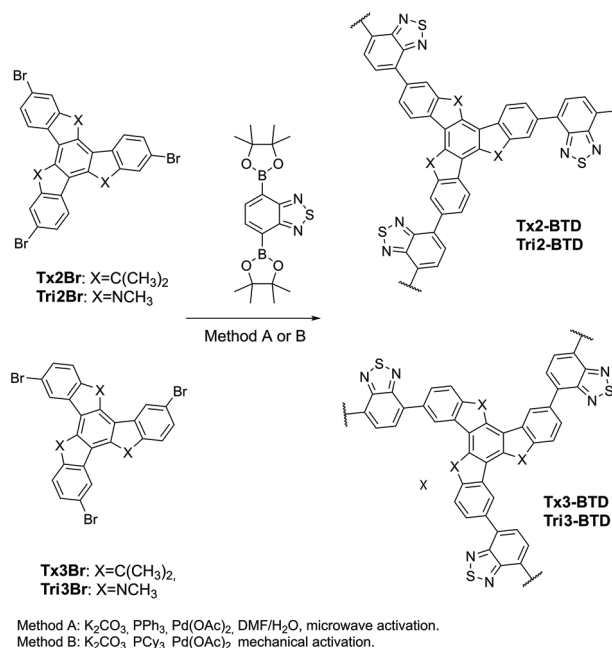
Scheme 1. Synthesis of **Tx2-BTD**, **Tx3-BTD**, **Tri2-BTD**, and **Tri3-BTD** CMPs based on truxene and triindole units.

good agreement with the expected theoretical value (Tables S1,S2, Supporting Information).

The FT-IR spectra of the four polymers are shown in **Figure 2a**. Truxene-based polymers show characteristic peaks ≈ 1600 and 2900 cm^{-1} corresponding to aromatic C=C and C–H stretches, typical signals of truxene skeleton vibrations whereas triindole-based polymers show peaks around 1720, 1610, and 2920 cm^{-1} corresponding to aromatic C=C, C–N and C–H stretches.
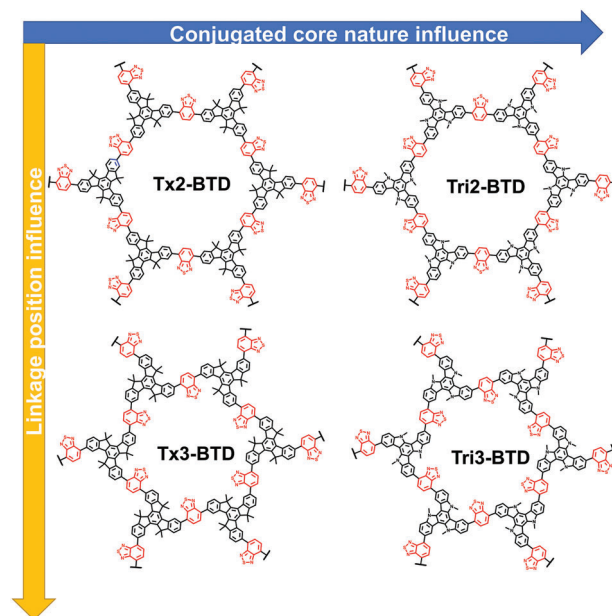

Figure 1. Idealized structures of **Tx2-BTD**, **Tx3-BTD**, **Tri2-BTD**, and **Tri3-BTD** CMPs with indication of the different parameter to study.
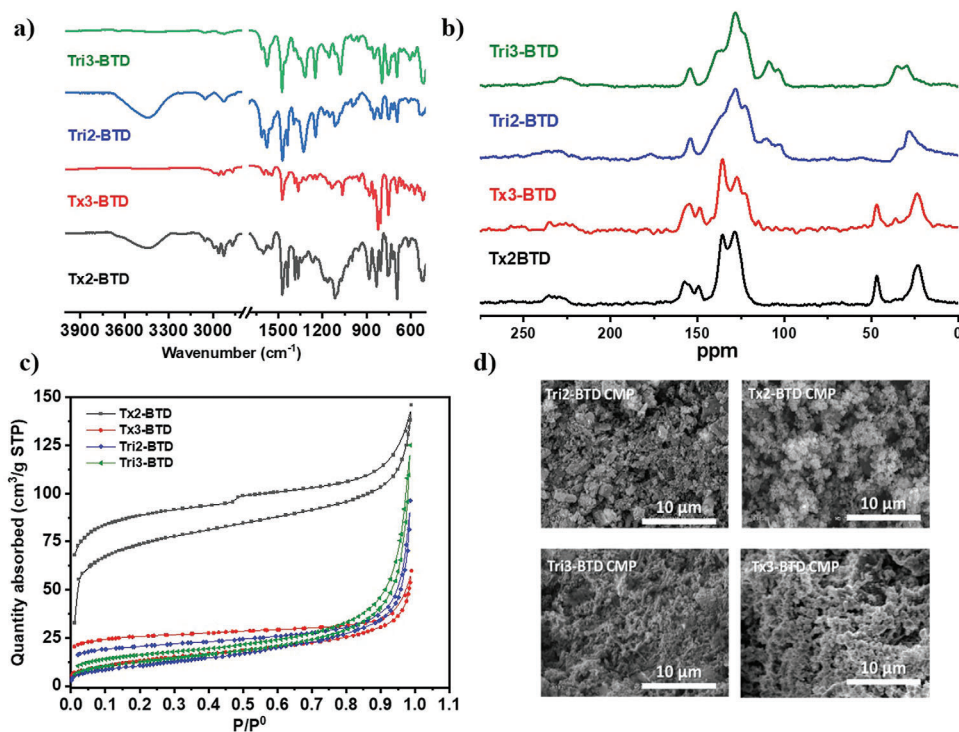
**ADVANCED
SCIENCE NEWS**

www.advancedsciencenews.com

**ADVANCED
FUNCTIONAL
MATERIALS**

www.afm-journal.de

Figure 2. Characterization data for truxene and triindole-based polymers: a) FT-IR, b) ^{13}C CP-MAS NMR, c) Nitrogen adsorption and desorption isotherms and d) SEM images.

The solid ^{13}C CP-MAS NMR spectra of truxene-based polymers (Figure 2b) present peaks at 23 and at 47 ppm ascribed to the methyl and the methylene carbons and peaks at 117 to 157 ppm assigned to the aromatic carbons of the truxene and BTD. On the other hand, triindole-based polymers present a signal at 28 ppm in the aliphatic region assigned to the methyl of NMe group signals in the aromatic region ranging from 102 to 154 ppm which are ascribed to the aromatic carbons of the triindole core and the BTD moiety.

All polymers showed high thermal stability (above 400°C) as determined by thermogravimetric analysis (TGA). (Figure S2, Supporting Information).

Porosity has been studied by isothermal nitrogen sorption measurements at 77 K. The specific surface areas show values of 270, 173, 46 and 40 $m^2 \cdot g^{-1}$ for **Tx2-BTD**, **Tx3-BTD**, **Tri2-BTD**, and **Tri3-BTD** CMPs as could be determined by Brunauer-Emmett-Teller (BET) method (Figure 2c). The lower specific surface areas found in the triindole based polymers are probably related to the high tendency of *N*-trimethyltriindole to self-assembly as has been extensively investigated previously,[26,27] and to the high steric hindrance imposed by the methyl groups of the truxene monomer, almost orthogonal to the plane of the molecule,[28] in contrast to the methyl groups of trindol, located almost coplanar to it.[26] In fact, we recently demonstrated through a computer-aided study that, while 2D polymers based on triindole show potential $\pi-\pi$ stacking, truxene-based polymers lead to more unstable configurations. This instability is attributed to physical steric impediment caused by the out-of-plane methyl groups of the truxene unit.[8] Pore size distributions were determined by DFT analysis (Figure S5 and Tables S3 and S4, Supporting In-

formation). Curiously the polymers obtained by mechanosynthesis show very similar characterization features, but their specific surface areas are however lower in all four cases (9, 18, 28, and 11 $m^2 \cdot g^{-1}$, respectively) (Figure S5, Supporting Information). We attribute these differences to a lower polymerization degree.

The morphology of the polymers was determined by field emission scanning electron microscopy (FE-SEM, Figure 2d). All four polymers show the formation of agglomerates of small particles with a globular shape characteristic of porous conjugated polymers.

2.2. Structural Features

With the main goal of exploring the structural differences exerted by the nature of the electron rich π-conjugated platform and the linkage position, the optimized ground-state structure of the four porous polymers were theoretically investigated using a canonical bottom-up approach. Initially, we performed a theoretical study of dimeric models in which two truxene or triindole units are linked with a benzothiadiazole unit through the two different positions under study (**Figure 3**). As can be observed, both heptacyclic triindole and truxene monomer led to similar internal disorder, however changing the linkage from 2,7,12 to 3,8,13 positions result in slightly more twisted structures, with increment of inter-ring dihedral angle values of 4° and 7° going from **Tx2-BTD** to **Tx3-BTD** and from **Tri2-BTD** to **Tri3-BTD**, respectively.

These molecular fragments were then sequentially assembled using periodic boundary conditions (PBC) to form larger subsystems, and 2D lattices were generated. For all the materials under
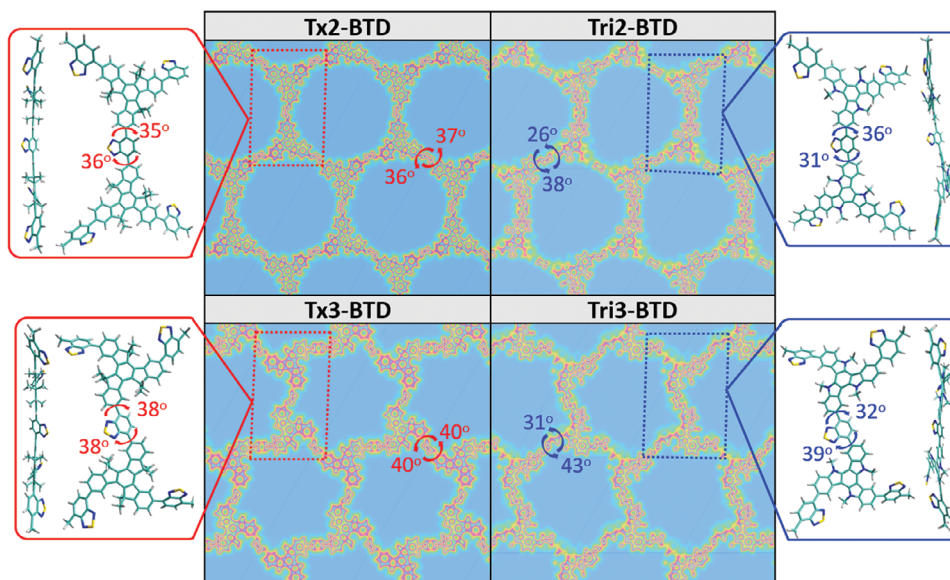
Figure 3. Top and lateral views of the DFT-optimized structures (PBE0/6-31G** level) for the dimeric models of the truxene (left) and triindole (right) polymers connected via the 2,7,12 (top) and 3,8,13 (bottom) positions. DFT-PBE-calculated surface charge density color maps in the xy-plane (at the z-position) for all the polymers under study are shown at the center. The dihedral angles between the heptacyclic cores and the BTD moieties (in absolute values) are also shown.

study, honeycomb-Kagome-like hexagonal lattices were observed, where the centers of the cores form a honeycomb sublattice and the connection between them exhibits an arrangement of a kagome sublattice.[29] As previously observed for the dimeric models, a slight improvement in planarity and thus electronic conjugation is predicted for the triindole-based polymers and for the 2,7,12 covalently linked polymers compared to the truxene-based and 3,8,13 linked polymers, respectively (Figure 3). It is important to highlight that our dimeric model calculations provide very accurate information on the molecular structures of 2D conjugated polymers.

2.3. Vibrational Properties

In order to investigate the influence of the nature of the C_3-symmetric monomers and the bond position on the effective conjugation length of these polymers, we have made use of Raman spectroscopy. It is well known that Raman spectroscopy provides valuable information about the electronic coupling between covalently connected conjugated moieties in organic semiconductors.[24,30] As shown in **Figure 4** the most intense Raman bands of the four polymers under study are located in the spectral region of 1500–1650 cm^{-1} and can be deconvoluted into three distinct peaks. With the help of DFT calculations, the different peak contributions are assigned to the same CC stretching mode (i.e., mode 8a of benzene)[31] but localized in different rings: (i) the Raman band at ≈1610 cm^{-1} (colored red) involves the outer benzene rings of the C_3 platform, (ii) the observed band at ≈1580 cm^{-1} (colored blue) corresponds to the inner benzene rings, and (iii) the band at ≈1544 cm^{-1} (colored orange) is located at the BTD linking units. The vibrational eigenvectors and the theoretical Raman spectrum (Figures S15–S17, Supporting In-

formation) support this assignment and confirm the good validity of our discussion. With these considerations, the experimental I_{1610}/I_{1580} intensity ratio can serve as a measure to estimate the effectiveness of the conjugation along the structures. As this ratio increases, the conjugation becomes more efficient.[24,30,32] If we compare the polymers having the same symmetric C_3 monomer we can clearly see that the intensity ratio is higher in the polymers connected through the 2,7,12 position than in those
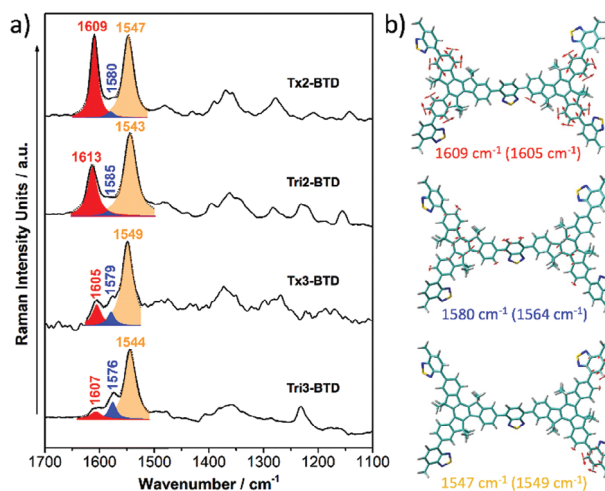

Figure 4. a) FT-Raman spectra for the four porous polymers under study in the solid state. Deconvolution of the 1500−1650 cm^{-1} Raman band into three distinct peaks based on Lorentzian fitting is shown. b) PBE0/6-31G** vibrational eigenvectors associated with the most outstanding C = C/C−C Raman features of **Tx2-BTD** taken as a representative example. The experimental and theoretical (in parentheses) wavenumbers are also shown.
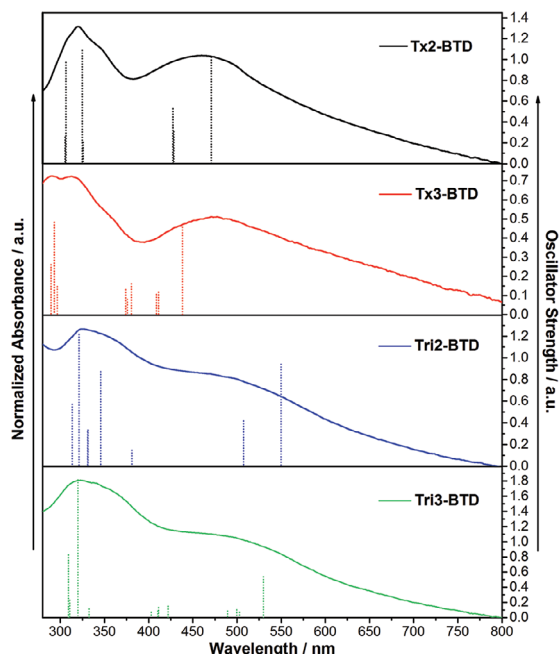
**ADVANCED
SCIENCE NEWS**

www.advancedsciencenews.com

**ADVANCED
FUNCTIONAL
MATERIALS**

www.afm-journal.de

Figure 5. Comparison between the experimental UV–vis absorption spectra of a) **Tx2-BTD**, b) **Tx3-BTD**, c) **Tri2-BTD** and d) **Tri3-BTD** porous polymers and TD-DFT calculated vertical excited-state transitions (dashed vertical bars) for their respective dimeric models at the PBE0/6-31G** level of theory.

connected through the 3,8,13 position, indicating more efficient conjugation in line with their less distorted structures. Interestingly, the band localized at ≈ 1544 cm^{-1} arising from the CC stretching mode of the BTD acceptor units is very sensitive to the electronic communication between truxene or triindole platforms, shifting toward lower frequency on going from **Tx3-BTD** (1549 cm^{-1}), **Tx2-BTD** (1547 cm^{-1}), **Tri3-BTD** (1544 cm^{-1}) to **Tri2-BTD** (1543 cm^{-1}) porous polymers. These results are in good accordance with those obtained in the electronic analysis, including the bandgap values detailed below.

2.4. Electronic Properties

The optical properties of these polymers were initially studied by UV–vis absorption and fluorescence spectroscopy and rationalized with the help of time-dependent density functional theory (TD-DFT) calculations. The absorption spectra of the four polymers in CH$_2$Cl$_2$ suspensions exhibit two principal absorption bands around 300 and 450–600 nm, respectively. High-energy transitions are associated with local π-π* excitations, as they are related to transitions between molecular orbitals located on the same π-conjugated molecular fragments. However, the lowest-energy electronic transitions involve a redistribution of the electron density between different molecular fragments (i.e., from the electron-rich $C3$ platforms toward the electron-deficient BTD group), thus involving intramolecular charge transfer (ICT) character (see Figures S9–S13, Supporting Information for more details). As can be observed in **Figure 5**, the nature of the π-conjugated platform influence on the optoelectronic properties, as triindole-based polymers present moderately red-shifted ab-

sorption spectra compared to their truxene-based counterparts. The connecting position shows only a weak influence on the optical properties, possibly due to the presence of the BTD acceptor group that favors electronic communication between the cores, although 2,7,12 covalently linked polymers displays more intense ICT transitions probably due to their less distorted structures further favoring the coupling between the BTD core and the C_3 platform. As seen in Figure 5 and Figure S9 (Supporting Information), TD-DFT vertical excitation energies reproduces very well the experimental data.

The solid-state diffuse reflectance spectra (UV-DRS) of the four polymers was recorded in order to estimate the HOMO−LUMO gap by the tauc plot obtained from Kubelka−Munk function (Figure S6, S7 in Supporting Information). As can be observed in **Figure 6a**, the band-gap values decrease when comparing triindole polymers to their truxene analogues and when going from 3,8,13 to 2,7,12-connected polymers, confirming previous trends in the effective conjugation evolution. DFT calculations correctly predict the experimental bandgap evolution within the series with the dimeric models overestimating the experimental values while the PBC calculations underestimate them.

Interestingly, theoretical calculations reproduce very well the influence of the two structural factors under study in the band
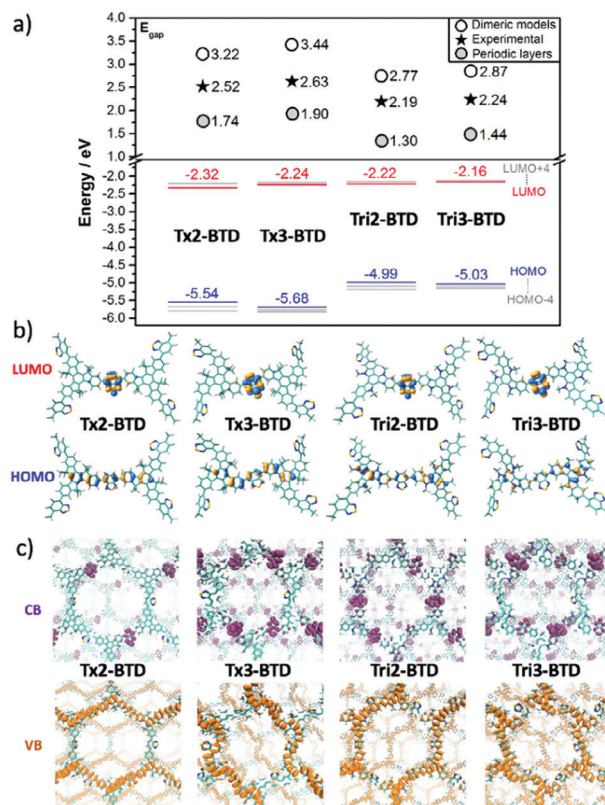

Figure 6. a) DFT-calculated molecular orbital energies (PBE0/6-31G** level) for the dimeric models of the polymers. The comparison between the experimental energy gaps and those calculated for dimeric models and periodic layers is also shown. b) Topologies of the HOMO and LUMO orbitals of the dimeric models. c) Topologies of the valence (VB) and conduction (CB) bands of the periodic layers.
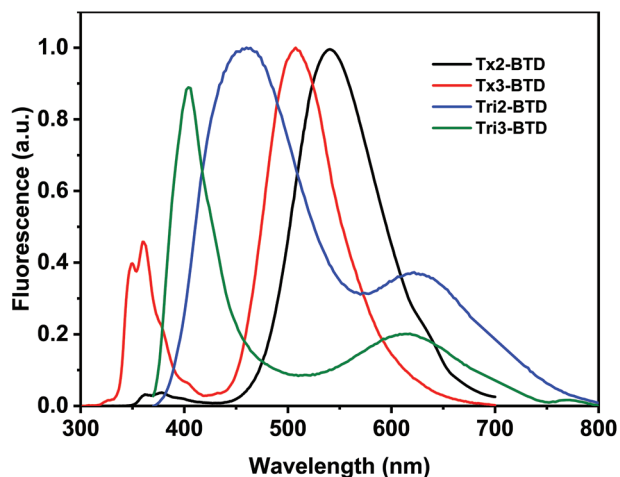
**ADVANCED
SCIENCE NEWS**

www.advancedsciencenews.com

**ADVANCED
FUNCTIONAL
MATERIALS**

www.afm-journal.de

Figure 7. Normalized experimental emission spectra of the four porous polymers under study.

Table 1. Quenching efficiencies (%) of polymers with PA, DNT, NB, and NT at 100 μM.

Polymer	Analyte			
	PA	DNT	NB	NT
Tx2-BTD	26.6	12.9	6.8	18.9
Tx3-BTD	74.0	45.0	36.6	59.2
Tri2-BTD	25.0	8.5	3.3	6.2
Tri3-BTD	33.0	6.8	6.7	5.5

gap evolution which results from a significant stabilization of the HOMO level and a slight destabilization of the LUMO level (which locates mainly on the BTD moiety) when going from triindole-based polymers to their truxene analogues and from the 3,8,13 to 2,7,12-connected polymers (Figure 6a). The band-gap narrowing going from **Tx2-BTD** (**Tx3-BTD**) to **Tri2-BTD** (**Tri3-BTD**) can be ascribed to the better extension of the π-conjugation observed in triindole-based polymers, where the valence band (VB) spreads over almost the whole π-conjugated framework (with exception of the BTD acceptor unit), whereas that of truxene-based systems are more localized in one selective direction (Figure 6a). On the other hand, the different linkage positions show a smoother impact on the π-electron delocalization between the cores which translate in the moderate increment of the band-gap when moving from 2,7,12 to 3,8,13-connected polymers.

The fluorescent spectra of the four polymers are characterized by two bands, which differ in intensity when we compare polymers containing the two different electron-rich units, with the low-energy band being the most intense in **Tx2-BTD** and **Tx3-BTD**, while the spectra of **Tri2-BTD** and **Tri3-BTD** polymers are dominated by the higher energy band (**Figure 7**). Moreover, the fluorescence spectra of triindole-based polymers are significantly red-shifted compared to those of the truxene-based polymers, in agreement with the evolution of the band-gap across the series. On the other hand, going from 2,7,12- to 3,8,13-linked polymers results in a clear red-shift in the truxene-based polymers but influences the triindole-based polymers to a lesser extent (Figure 7).

2.5. Sensing of Explosives

In an attempt to advance toward practical applications we have investigated the performance of these polymers in the detection of analytes of interest as explosives and nitro aromatic compounds, one of most promising applications of π-conjugated porous polymers.[5] In particular, we have evaluated the potential use of these truxene and triindole-based polymers for the detection of explosives such as picric acid (**PA**), and nitroderivatives

including 2,4-dinitrotoluene (**DNT**), *p*-nitrotoluene (**NT**) and *p*-nitrobenzene (**NB**).

In an initial experiment to assess the response of the four polymers in the presence of the different nitroaromatic compounds, a constant concentration of each analyte (100 μM) was added and the corresponding quenching efficiency (QE) was determined (**Table 1** and **Figure 8**). The emission of all four polymers is significantly affected by **PA**. Triindole-based **Tri2-BTD** and **Tri3-BTD** polymers present very similar performance with QE ≈ 30% for **PA** and much lower responses for the rest of the investigated nitroaromatic compounds. The differences between the two truxene-based polymers are much more significant. Although quenching efficiencies follow similar trends (**PA > NT > DNT > NB**) the values are significantly higher for **Tx3-BTD**.

To quantify the quenching behavior, the polymer suspensions were titrated with increasing amounts (0−350 μM) of the different nitroaromatics and the data were analyzed using the Stern−Volmer equation $I_0/I = 1+ K_{SV}[Q]$. Calculated constants (K_{Sv}) of 25.5×10^3, 10.2×10^3, 10.2×10^3, and 11.5×10^3 M^{-1} could be determined for **Tx3-BTD** in the presence of **PA**, **DNT**, **NB**, an **NT**, respectively (**Table 2** and Figures S18 and S19, Supporting Information).[5,33,34] These results do not follow the
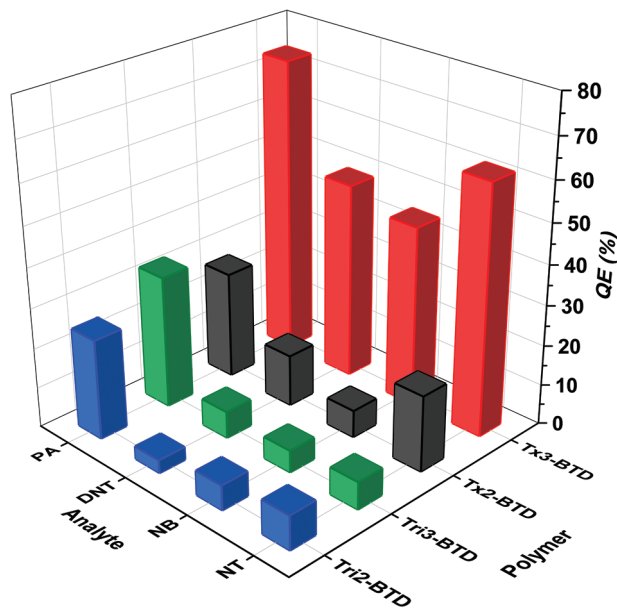

Figure 8. Quenching efficiencies of porous polymers in the presence of **PA**, **DNT**, **NB**, and **NT** at 100 μM.

Table 2. Stern−Volmer Constants ($\times 10^3$ M^{-1}) and Detection Limits (LOD) of polymers with PA, DNT, NB, and NT.

Polymer	Analyte							
	PA		DNT		NB		NT	
	K_{SV}[a]	LOD[b]	K_{SV}[a]	LOD[b]	K_{SV}[a]	LOD[b]	K_{SV}[a]	LOD[b]
Tx2-BTD	2.4	4.7	2.4	4.7	–	–	2.2	5.0
Tx3-BTD	25.5	1.6	10.2	3.4	10.2	3.2	11.5	3.0
Tri2-BTD	6.1	4.3	–	–	–	–	–	–
Tri3-BTD	4.8	4.4						

[a] The value of KsV was ($\times 10^3$ M^{-1}) and [b] the units of LOD were (µM).

expected trends on the basis of a photoinduced electron transfer (PET) mechanism, which would predict higher K_{sv} values with an increasing difference between the LUMO levels of the polymer and the fluorophores: **PA > DNT > NB > NT** (See Figure S20, Supporting Information). Particularly for NT and DNT, significant differences in LUMO level energy are expected, yet they exhibit similar K_{sv} values. However, there is a significant match of this trend, with the amplitude of the spectral overlap between the absorption of the nitroaromatic compounds and the fluorescence of the polymers, pointing to a resonance energy transfer mechanism (RET). Nevertheless, a contribution of a Photoinduced Electron Transfer (PET) mechanism cannot be ruled out. The high selectivity toward **PA** exhibited by the triindole-based polymers can be explained by considering a similar explanation: In fact, due to their more red-shifted emission only **PA** shows some spectral overlap (Figure S21, Supporting Information).

2.6. Photocatalytic Activity

Considering the good photocatalytic activity previously shown by truxene-based polymers[21–23] we have explored their potential interest in the photocatalytic detoxification of chemical agents such as the mustard gas (MG). Experiments were performed on the less toxic simulant 2-chloroethyl ethylsulfide (MGS) under blue LED light and an oxygen balloon (**Scheme 2**). Experimental details can be found in the supplementary material. Results show that only truxene-polymers effectively catalyzed the reaction with **Tx2-BTD** being the most efficient as it selectively leads to the sulfoxide in only two hours (**Table 3**, entry 1 and Figure S21, Supporting Information). At this time polymer **Tx3-BTD** shows much lower conversion (27%) while **Tri2-BTD** and **Tri3-BTD** do not react (entries 3 and 4). Experiments with light in the absence of catalyst do not lead to the product (entry 5); on the other hand, only traces of product were detected in the dark (entry 6), indicating that both light and catalyst were necessary to promote the electron transfer.
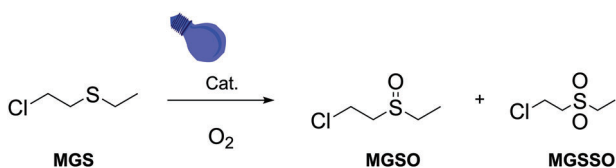
Scheme 2. Photooxidation of mustard gas.

The recyclability and photochemical stability of **Tx2-BTD** was also evaluated using MGS as substrate, under oxygen atmosphere and blue LED light irradiation (Figure S23, Supporting Information). After each run, a new substrate was added to the reaction mixture and irradiated again. As can be observed, the activity and selectivity were maintained for at least seven consecutive runs.

Generally, the application of porous organic polymers as photocatalysts for oxidation reactions involves two reactive species:[35–37] singlet oxygen ($^1O_2$) and a superoxide radical anion ($O_2^{\bullet-}$). In order to identify the primary active species involved in this photocatalytic process, we have investigated the photooxidation of MGS by **Tx2-BTD** in the presence of potassium iodide KI (10 mmol. L^{-1}), sodium azide NaN$_3$ (10 mmol. L^{-1}) and benzoquinone BQ (1 mmol. L^{-1}) as holes, $^1O_2$ and $O_2^{\bullet-}$ scavengers respectively. The conversion decreases drastically in all three cases indicating that singlet oxygen, superoxide radical anion and hole are implied in this reaction confirming the previously proposed mechanism, as shown in **Figure 9**. The ability of this compound to generate $^1O_2$ was further confirmed in the selective photooxygenation of α-terpinene into ascaridole, involving a [4 + 2] cycloadditions with $^1O_2$ (see Figure S24, Supporting Information).[38,39]

The differences in the reactivity shown by the four polymers can be understood on the basis of their different

Table 3. Photo-oxidation of mustard gas simulant (MGS).[a]

Entry	Catalyst	Yield [%]	Selec. [%]
1	**Tx2-BTD**	>98	100
2	**Tx3-BTD**	27	100
3	**Tri2-BTD**	0	–
4	**Tri3-BTD**	0	–
5	none	0	–
6	**Tx2-BTD**[b]	traces	
7	**Tx2-BTD**[c]	4	0
8	**Tx2-BTD**[d]	2	3
9	**Tx2-BTD**[e]	0	0

[a] Reaction conditions: Polymer (1.5 mg), MGS (0.05 mmol), MeOD (0.5 mL), O$_2$ (1 atm), Blue LED lamp (18 W, 470 nm), 25°C, 2 h; [b] Dark; [c] In the presence of NaN$_3$ (0.25 mmol); [d] In the presence of KI (0.025 mmol); [e] In the presence of p-benzoquinone (0.05 mmol).

ADVANCED
SCIENCE NEWS

www.advancedsciencenews.com

ADVANCED
FUNCTIONAL
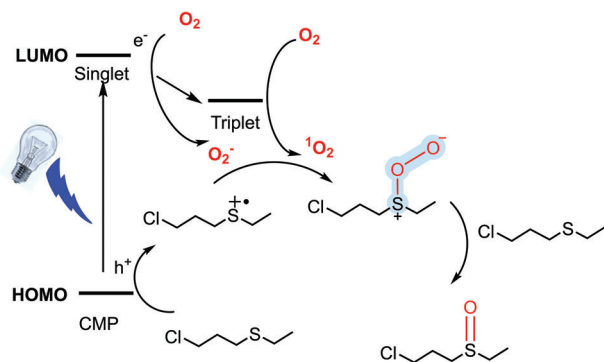**MATERIALS**

www.afm-journal.de

Figure 9. Proposal of a mechanism for the photooxidation of MSG.

HOMO and LUMO levels. When light is absorbed, an electron from the HOMO is excited to the LUMO, creating an electron-hole pair. The narrower HOMO-LUMO gap found in triindole-based polymers should increase the light absorption resulting in larger photocatalytic activity and minimize electron-hole recombination as previously reported in other donor-acceptor porous polymers.[40] However, the higher HOMO energy levels of these materials will reduce their ability to donate electrons. This implies a decreased tendency for oxidation, likely inhibiting the generation of the sulfide cation radical.

3. Conclusion

In conclusion, we have synthesized four novel donor-acceptor (D-A) porous polymers by combining two electron donor types (truxene and triindole) with an electron-deficient monomer (benzothiadiazole) through two different positions (2,7,13 or 3,8,13). Their optoelectronic properties were studied by theoretical and experimental methods and it was found that the electronic character of the connectivities exerts a strong influence on the HOMO and LUMO energy levels. As a result of this study, a polymer exhibiting remarkable sensing capabilities for explosive TNT has been identified. Furthermore, a polymer capable of efficiently photocatalysing the aerobic sulfoxidation of the sulfur mustard simulant 2-chloro-ethyl ethyl sulfide has been developed, highlighting the potential interest of these polymers in defense-related applications. The structure-performance relationships observed among the four polymers have enabled us to deepen our understanding of the mechanisms underlying the performance of these polymers in the aforementioned applications, thereby providing valuable information for the enhancement of their properties. The results of this study highlight the importance of tuning the band structure and optimizing the material's electronic properties to match the specific ones and show how subtle differences in the polymers can drive to drastic differences in the performance of these materials.

Supporting Information

Supporting Information is available from the Wiley Online Library or from the author.

Conflict of Interest

The authors declare no conflict of interest.

Data Availability Statement

The data that support the findings of this study are available in the supplementary material of this article.

[1] D. J. Klapec, G. Czarnopys, J. Pannuto, *Forensic Sci. Int. Synerg.* **2020**, *2*, 670.
[2] J. S. Caygill, F. Davis, S. .J. Higson, *Talanta* **2012**, *88*, 14.
[3] J. S. M. Lee, A. I. Cooper, *Chem. Rev.* **2020**, *120*, 2171.
[4] D. Taylor, S. J. Dalgarno, Z. Xu, F. Vilela, *Chem. Soc. Rev.* **2020**, *49*, 3981.
[5] S. Wang, H. Li, H. Huang, X. Cao, X. Chen, D. Cao, *Chem. Soc. Rev.* **2022**, *51*, 2031.
[6] X. Liu, Y. Xu, D. Jiang, *J. Am. Chem. Soc* **2012**, *134*, 8738.
[7] H. Zhang, W. Wei, K. A. I. Zhang, *Chem. Commun.* **2023**, *59*, 9167.
[8] S. Gámez-Valenzuela, M. Echeverri, B. Gómez-Lor, J. I. Martínez, M. C. Ruiz Delgado, *J. Mater. Chem. C* **2020**, *8*, 15416.
[9] A. Uslu, S. O. Tümay, S. Yeşilot, *J. Photochem. Photobiol. C* **2022**, *53*, 100553.
[10] L. A. Panther, D. P. Guest, A. McGown, H. Emerit, R. K. Tareque, A. Jose, C. M. Dadswell, S. J. Coles, G. J. Tizzard, R. González-Méndez, C. A. I. Goodall, M. C. Bagley, J. Spencer, B. W. Greenland, *Chem. - Eur. J.* **2022**, *28*, 202201444.
[11] T. Seo, N. Toyoshima, K. Kubota, H. Ito, *J. Am. Chem. Soc.* **2021**, *143*, 6165.
[12] K. Kubota, E. Baba, T. Seo, T. Ishiyama, H. Ito, *J. Org. Chem.* **2022**, *18*, 855.
[13] K. Yoo, S. Fabig, S. Grätz, L. Borchardt, *Faraday Discuss.* **2023**, *241*, 206.
[14] R. Takahashi, T. Seo, K. Kubota, H. Ito, *ACS Catal.* **2021**, *11*, 14803.
[15] Q. Lemesre, T. Wiesner, R. Wiechert, E. Rodrigo, S. Triebel, H. Geneste, *Green Chem.* **2022**, *24*, 5502.
[16] F. Effaty, X. Ottenwaelder, T. Friščić, *Curr. Opin. Green Sustain. Chem.* **2021**, *32*, 100524.

[17] A. Krusenbaum, S. K. Hinojosa, S. Fabig, V. Becker, S. Grätz, L. Borchardt, *Phys. Chem. Chem. Phys.* **2023**, *25*, 16781.

[18] E. Troschke, S. Grätz, T. Lübken, L. Borchardt, *Angew. Chem Int. Ed.* **2017**, *56*, 6859.

[19] J.-S. M. Lee, T. Kurihara, S. Horike, *Chem. Mater.* **2020**, *32*, 7694.

[20] A. Krusenbaum, J. Geisler, F. J. L. Kraus, S. Grätz, M. V. Höfler, T. Gutmann, L. Borchardt, *J. Polym. Sci.* **2022**, *60*, 62.

[21] S. Gharbi, N. Méndez-Gil, K. Hriz, M. Majdoub, B. Gómez-Lor, *ACS Appl. Polym. Mater.* **2023**, *5*, 2359.

[22] A. Valverde-González, C. G. López Calixto, M. Barawi, M. Gomez-Mendoza, V. A. de la Peña O'Shea, M. Liras, B. Gómez-Lor, M. Iglesias, *ACS Appl. Energy Mater.* **2020**, *3*, 4411.

[23] J. Guadalupe, A. M. Ray, E. M. Maya, B. Gómez-Lor, M. Iglesias, *Polym. Chem.* **2018**, *9*, 4585.

[24] M. Echeverri, S. Gámez-Valenzuela, R. C. González-Cano, J. Guadalupe, S. Cortijo-Campos, J. T. López Navarrete, M. Iglesias, M. C. Ruiz Delgado, B. Gómez-Lor, *Chem. Mater.* **2019**, *31*, 6971.

[25] Y. Kim, S. Das, S. Bhattacharya, S. Hong, M. G. Kim, M. Yoon, S. Natarajan, K. Kim, *Chem. - Eur. J.* **2012**, *18*, 16642.

[26] E. M. García-Frutos, E. Gutierrez-Puebla, M. A. Monge, R. Ramírez, P. de Andrés, A. de Andrés, R. Ramírez, B. Gómez-Lor, *Org. Electron.* **2009**, *10*, 643.

[27] A. Benito-Hernández, U. K. Pandey, E. Cavero, R. Termine, E. M. García-Frutos, J. L. Serrano, A. Golemme, B. Gómez-Lor, *Chem. Mater.* **2013**, *25*, 117.

[28] T. Ogaki, E. Ohta, Y. Oda, H. Sato, Y. Matsui, M. Kumeda, H. Ikeda, *Asian J. Org. Chem.* **2017**, *6*, 290.

[29] C. Barreteau, F. Ducastelle, T. Mallah, *J. Condens. Matter Phys.* **2017**, *29*, 465302.

[30] C. Ruiz, J. T. López Navarrete, M. C. Ruiz Delgado, B. Gómez-Lor, *Org. Lett.* **2015**, *17*, 2258.

[31] E. B. Wilson, J. C. Decius, P. C. Cross, B. R. Sundheim, *J. Electrochem. Soc.* **1955**, *102*, 9.

[32] S. Gámez-Valenzuela, A. Benito-Hernández, M. Echeverri, E. Gutierrez-Puebla, R. P. Ortiz, M. C. Ruiz Delgado, B. Gómez-Lor, *Molecules* **2022**, *27*, 1121.

[33] K. Wang, T.-M. Geng, H. Zhu, C. Guo, *Microporous Mesoporous Mater.* **2024**, *363*, 112794.

[34] W. He, J. Duan, H. Liu, C. Qian, M. Zhu, W. Zhang, Y. Liao, *Prog. Polym. Sci.* **2024**, *148*, 101770.

[35] G. Kumar, B. Cai, S. Ott, H. Tian, *Chem. Phys. Rev.* **2023**, *4*, 011307.

[36] Y. Gao, H. Xu, S. Zhang, Y. Zhang, C. Tang, W. Fan, *Org. Biom. Chem.* **2019**, *17*, 7144.

[37] X. Chen, K. Deng, P. Zhou, Z. Zhang, *ChemSusChem* **2018**, *11*, 2444.

[38] A. Li, C. Tan, T. Yuan, J. Liang, D. Gao, Y. Tan, Y. Jiang, *J. Mater. Chem. A* **2018**, *6*, 15927.

[39] Y. Zhi, Z. Yao, W. Jiang, H. Xia, Z. Shi, Y. Mu, X. Liu, *ACS Appl. Mater. Interfaces* **2019**, *11*, 37578.

[40] Y. S. Kochergin, D. Schwarz, A. Acharjya, A. Ichangi, R. Kulkarni, P. Eliášová, J. Vacek, J. Schmidt, A. Thomas, M. J. Bojdys, *Angew. Chemie – Int. Ed.* **2018**, *57*, 14188.

2316754 (9 of 9)